Modelling the Positional and Orientation Sensitivity of Inductively Coupled Sensors for Industrial IoT Applications

Richard McWilliam and Alan Purvis
School of Engineering and Computing Sciences
Durham University
Durham, United Kingdom
e-mail: r.p.mcwilliam@durham.ac.uk

Samir Khan
School of Mechanical, Automotive and Aerospace
Engineering, Coventry University
Coventry, United Kingdom
e-mail: samir.khan@coventry.ac.uk

***Abstract*— As the Internet of Things (IoT) sector continually expands there is a growing abstraction between physical objects and the data associated with them. At the same time, emerging Industrial-IoT applications rely upon diverse and robust hardware sensing interfaces in order to deliver high quality data. In this paper, the fundamental limitations associated with inductive proximity sensing interfaces are considered in terms of positional and orientation sensitivity and a triaxial approach is proposed that enables arbitrary source-sensor positioning. A matrix transformation model based on the field coupling equations is applied to a number of candidate configurations assessed according their relative source-sensor coverage and graphical visualization of coupling quality. Particular attention is paid to the recombination of tri-sensor outputs involving direct-summation, rectify-summation, best-coil and root-mean-square methods. Of these, the rectify-summation method was observed to provide favorable performance, exceeding 70% coverage for practical cases, thus far exceeding that of traditional co-planar arrangements.**

***Keywords- Internet of things; Industrial sensing; Radio frequency identification; Inductive coupling*.**

I. INTRODUCTION

The past five years have witnessed a proliferation of technological innovations within major industrial services platforms [1] and advancements in economic policies for key sectors such as food industries [2] that utilize traditional RFID tracking and logistics devices. However, despite the attractive prospects offered by emerging IIoT markets, technological limitations of physical hardware sensor layers are not well enough understood. There exist a number of opportunities to extend the reach of identification and monitoring sensors towards the edge of IIoT cyber-physical boundaries by incorporating more compact and robust physical interfaces supporting integrated environmental sensing and identification whilst remaining tolerant to dynamic position and orientation conditions. At the higher sensor network and information layers, including big data processing and emerging Physical-Cyber-Social (PCS) infrastructures [3], applications will rely not only upon novel back-end services, but also high-quality sensor data if the volume of data is to be reduced to manageable levels.

The shift towards industrial servitization is compelling organizations to deliver guaranteed system availability and major savings in the cost of through-life product support [4]. Sensory data analysis strategies for through-life system care is complex, but can yield significant cost savings and progress towards zero-downtime of maintenance-driven products [5]. This strategy calls upon strong M2M and P2M interactivity throughout system life cycle and warrants an increasing use of "digital labor" in the form of smart sensors, sophisticated M2M communications [6], cloud-based acquisition and processing [7] and algorithms for automated control and monitoring of system performance that make best use of available sensor coverage [8]. At the widest socio-political levels, the development of novel embedded sensors that are robust and dependable will help underpin the uptake and social trust of future large-scale IIoT initiatives such as Smart Cities [9] and global IoT systems that utilize a multitude of existing and emerging sensor technologies [10].

However, in order to meet long-term industrial requirements for data acquisition, the limitations of sensor positioning and orientation sensitivity of the interfacing device must be further explored [11]. With recent innovations in IoT, many researchers are now concentrating their efforts on developing universal acquisition interfacing and specialised IoT sensors [12], [13]. It is therefore necessary to understand the properties of source-sensor coupling for the design of these measurement devices. Likewise, it is also important to find a compromise between the data rate, resolution and accuracy of the IIoT application.

By focusing on the above issue, this paper aims to study the particular problem of modelling the free-space orientation model for power and communication is proposed based on tri-axial source and triaxial sensor coils. Such arrangements are becoming feasible through advances in 3D additive manufacturing technologies capable of integrating conductive tracks and integrated circuits within the mechanical assembly. Several radial coil source/sensor combinations are studied in terms of their impact on sensor coverage defined over the shell of a unit sphere.

II. SENSOR POSITION AND ORIENTATION SENSITIVITY

Traditional proximity RFID transponders and sensors are based on a single source and sensor coil arrangement (Fig. 1)

whereby power and communications is supported by inductive coupling. Restrictions associated with proximity-coupling arise from the use of singular planar coils that must be arranged in a mutually co-planar fashion; otherwise a rapid reduction of coupling occurs that inhibits further communication. At the same time, it is well known that the inherently localized nature of near-field contact-less sensing mature in traditional IoT applications offers an inherent security 'zone' for sensitive assets. However, its integration within IIoT is less clear due to the orientation sensitivity and power transfer efficiency.

Even for the optimal case of co-planarity, the received power is proportional to d^{-6}, where d is the source-sensor coil separation, representing a punitive distance fall-off characteristic that is further exacerbated when co-planarity is lost [14]. While this limitation has been manageable within certain RFID applications, it is inherently restrictive for emerging IIoT applications including large-scale wireless power transfer systems [15]. Further field dampening effects are caused by the presence of foreign materials, further compounding the need for careful pre-planning and prediction of the expected coupling geometry. As a result of this, current IIoT data collection and processing platforms still tend to utilize hard-wired platforms and discrete integrated sensors [16].

In this paper, an orientation-flexible sensing and communication interface is proposed that uses multiple coupling coils in order to reduce the dependency on co-planarity. The concept is underpinned by the recent advances in 3D additive manufacturing technologies capable of integrating conductive tracks and integrated circuits within the mechanical assembly. By introducing tri-coil arrangements, whereby *X*-, *Y*- and *Z*-oriented coils are superimposed, a greater freedom of position and orientation becomes possible. The approach is analysed in terms of a magnetic coupling model for near-field power and communications (NFPC) sensors evaluated over the shell of a unit sphere that serves to represent the possible degrees of positional and orientation freedom of the sensor. Several sensor recombination methods are studied in terms the specified sensor movement and threshold coupling in order to determine their positional coverage i.e., over which power and communications is possible.

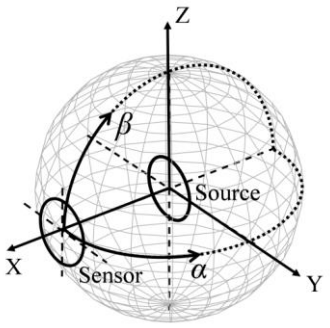

Figure 1. Geometry of single source and single sensor coils when oriented in the *X*-direction and restricted to the shell of a unit sphere. Sensor position is described on unit sphere by angular variables (α,β).

A. Data quality and availability

Within the IIoT context, data gathering and quality considerations have primarily focused on:

- improving operational efficiency or availability through predictive maintenance of engineering systems and their remote management [2], [17];
- smart monitoring using sensors, analytics and Internet-enabled connections. The monitoring of mechatronic systems and software is of particular importance here, as evidenced in the recent literature [18]–[20];
- enhanced P2M interoperability and awareness for emerging applications such as healthcare [21].

Two related aspects that have become prominent in this context are sub-component complexity and data availability [7]. Component complexity relates to the number of system components that generally vary within different application environments and from one implementation to another. In many cases the control and management of complex systems and sub-systems requires an effective use of available sensory data or else the integration of new and novel embedded sensors. Qualitative and quantitative data reasoning was studied by Li *et al.* [22] wherein a method was proposed to characterize incomplete and qualitative data and hence improve management of design complexity. A method of self-managed real-time monitoring of variations in industrial control systems was proposed in [23] that involved the use of intelligent cyber sensors employed to ensure the defined security requirements and the controllability of system complexity.

With respect to data availability, IIoT infrastructures will need to optimize their use of system resources to achieve higher efficiency and lower operational cost [24]. An example of this is the smart monitoring of energy networks, in which significant investment is needed to furnish existing and future power storage and conversion networks with highly localized control and monitoring that must be robust and secure [25]. Future advancements in this area of IIoT require especially robust sensory data collection networks. Even though IIoT is becoming mainstream there remains a number of barriers that must be overcome in order to realise IIoT interoperability, security and hardware sensor technologies [26]. The successful IIoT application should be capable of supporting system level decision-making within complex designs. Furthermore, interface sensors for IIoT will be expected to acquire data from environments exhibiting variable coupling, resolution and dynamic range.

III. PROXIMITY SENSING AND INDUSTRIAL IOT

Although there are similarities between I-IoT and the comparatively mature IoT infrastructures that exist in e-commerce ticketing and product supply chains [14], there are fundamental differences with respect to the expected robustness and availability of industrial hardware platforms that must be dependable within confined and harsh operational environments. It is well known that the inherently localized nature of near-field contactless sensing offers an inherent security 'zone' for sensitive assets as well as orientation detection [27]. A core challenge is the energy efficiency of IoT sensor networks that directly affects the Quality of Service (QoS) in industrial applications [1]. Energy efficiency may optimized through network protocols [17], RF chip design [28] and coupling efficiency. For proximity sensing, coupling efficiency is affected by both orientation and the surrounding environment [29].

Proximity I-IoT sensing hardware extends far beyond existing e-commerce domains found in IoT and there are many opportunities for innovation in this sector. For example, sensor networks for jet engine test beds must survive high temperature and vibration conditions whilst providing high data bandwidth telemetry during test.

Traditional proximity sensors utilise a single source and sensor coil arrangement, whereby power and communications are supported by co-planar inductive coupling. This arrangement is depicted in Fig. 1 where the sensor position lies on the shell of a sphere of radius r and the received power to source-sensor separation, d, decays according to d^{-6}. While this arrangement has become the standard interface for proximity sensing [15], coupling efficiency is highly dependent upon orientation.

Non-planar coil arrangements have been proposed to reduce orientation sensitivity by fabricating embedded orthogonal tracks within the sensor volume [30], [31]. However, it is still difficult to predict their performance within confined packaging and dampening effects caused by the presence of foreign materials further compounding the need for careful pre-planning and prediction of the expected coupling geometry. For this reason, the coupling efficiency of simpler triaxial coil arrangements is considered here.

IV. PHYSICAL COUPING MODEL

Proximity coupling is modelled as a inductive source-sensor arrangement as depicted in Fig. 1. For the case shown, the transmitting and receiving coils are nominally arranged such their respective magnetic moments are aligned i.e., the coils are co-planar oriented along the x-axis. It has been assumed that the coil radius a is considerably smaller than the coil separation r (or more strictly $a^2 < r^2$). With reference to Fig. 2, mutual interaction occurs between the magnetic field components of each coil, which are described according to the radial and tangential field equations:

$$H_r = \frac{M}{r^3}\cos\beta \qquad H_t = \frac{M}{2r^2}\sin\beta \qquad M = \frac{a^2 IN}{2} \tag{1}$$

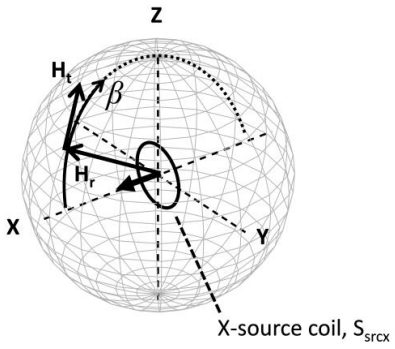

Figure 2. Basic coordinate system showing X-oriented source coil.

where H_r and H_t are the radial and tangential field components respectively, β is the angle of elevation between the magnetic moment vector and position of observation, I is the magnitude of alternating current passing through each coil and N is the number of coil turns.

A. Orthogonal and Co-planar Coil Arrangement

Considering initially a single source and sensor coil pair, three orthogonal arrangements are considered as illustrated in Fig. 3(a-c). The source coil assumes a fixed position oriented along the x-axis and is referred to as an X-source coil. Adopting similar nomenclature for the sensor coil, each of the X, Y- and Z-sensor coil orientations can be seen. Clearly mutual coupling exists only for the case of X-sensor (radial coupling); while other combinations experience zero coupling due to orthogonality. Thus, each of the co-planar and orthogonal cases can be represented by the coupling equation:

$$\boldsymbol{S_{out}} = \frac{M}{r^3}\begin{bmatrix}1 & 0 & 0\\ 0 & -0.5 & 0\\ 0 & 0 & -0.5\end{bmatrix}\boldsymbol{S_{src}} = \frac{M}{r^3}\boldsymbol{O}\boldsymbol{S_{src}} \tag{2}$$

where $\boldsymbol{O}$ is a constant matrix termed the orientation matrix and the input and output coil signals are written in vector form:

$$\boldsymbol{S_{src}} = \begin{bmatrix}S_{srcx}\\ S_{srcy}\\ S_{srcz}\end{bmatrix},\ \boldsymbol{S_{out}} = \begin{bmatrix}S_{outx}\\ S_{outy}\\ S_{outz}\end{bmatrix} \tag{3}$$

Referring again to Fig. 1, (2) describes the combined coupling between three orthogonal source coils placed at the origin of a unit sphere ($r = 1$) and three orthogonal sensor coils placed on the x-axis at $x = 1$. Since $\boldsymbol{O}$ is a diagonal matrix, orthogonal source/sensor pairs contribute zero coupling, while co-planar pairs contribute radial or tangential field coupling.

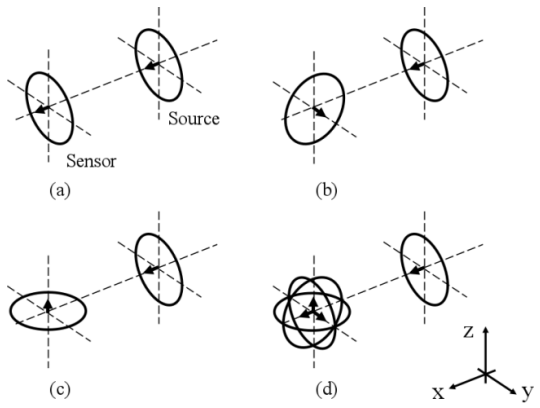

Figure 3. Example X-source coil and various sensor coil orientations. (a) X-sensor. (b) Y-sensor. (c) Z-sensor. (d) Tri-sensor.

B. Influence of Sensor Position and Orientation

The matrix representation (2) permits the inclusion of additional source-sensor contributions that arise when the sensor position and orientation is no longer confined to the *x*-axis. Depending on the application requirements, the sensor coil ensemble may be expected to change position or orientation relative to the source ensemble, in which case the expected variations of coupling must be known. Sensor position is accounted for by azimuthal (α) and elevation (β) angles (see Fig. 1) while sensor orientation is described according to azimuthal (ψ) elevation (θ) and roll (ϕ) rotations (see Fig. 4). Single, dual- or tri-source and sensor coils ensembles are handled by assigning or evaluating the respective elements of vectors (3). If the co-planar arrangements of Fig. 3 are imposed, then only azimuth and elevation rotation need be considered while roll rotation must be included when dual- or triaxial coils are used.

Given the above description, the problem may then be generalized by applying the method of Raab *et al*. [32] for positional and orientation transformation, wherein a sequence of positional and rotational transformations are applied to the orientation matrix ***O***:

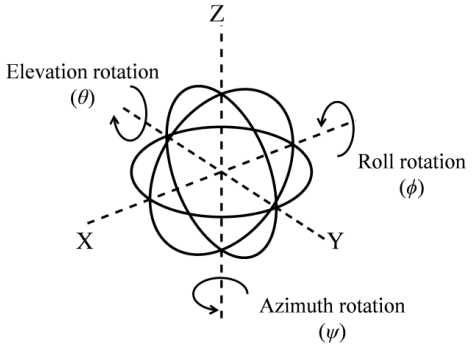

Figure 4. Rotation geometry for orthogonal sensor arrangements.

$$\text{(Azimuth position)}\quad T_\alpha = \begin{bmatrix} cos\alpha & sin\alpha & 0 \\ -sin\alpha & cos\alpha & 0 \\ 0 & 0 & 1 \end{bmatrix}$$

$$\text{(Elevation position)}\quad T_\beta = \begin{bmatrix} cos\beta & 0 & -sin\beta \\ 0 & 1 & 0 \\ sin\beta & 0 & cos\beta \end{bmatrix}$$

$$\text{(Azimuth rotation)}\quad T_\psi = \begin{bmatrix} cos\psi & sin\psi & 0 \\ -sin\psi & cos\psi & 0 \\ 0 & 0 & 1 \end{bmatrix}$$

$$\text{(Elevation rotation)}\quad T_\theta = \begin{bmatrix} cos\theta & 0 & -sin\theta \\ 0 & 1 & 0 \\ sin\theta & 0 & cos\theta \end{bmatrix}$$

$$\text{(Roll position)}\quad T_\phi = \begin{bmatrix} 1 & 0 & 0 \\ 0 & cos\phi & sin\phi \\ 0 & -sin\phi & cos\phi \end{bmatrix} \tag{4}$$

The aggregate sensor output is then determined by the expression:

$$S_{out} = \frac{M}{r^3} f_o(\psi, \theta, \phi) f_p(\alpha, \beta) S_{src} \tag{5}$$

where the transformations:

$$f_p = T_{-\alpha} T_{-\beta} O T_\beta T_\alpha, f_o = T_\phi T_\theta T_\psi \tag{6}$$

account for sensor position and orientation respectively.

The application of transformation operation successively alters the orientation matrix to account for sensor position and orientation, after which a final transformation of the form (2) yields $\boldsymbol{S_{out}}$. Azimuthal and elevation position are accounted for by a two-step transformation process, in which forward/reverse transformations of an equivalent source coil aligned to the sensor coil takes places, while the polarities of the α, β indicies determine the direction of transformation [32]. Except for the simple orthogonal arrangements considered in (2), the transformation matrices create new contributions within the non-diagonal elements of ***O***.

From the above model, the quality of mutual coupling in each of the *x*-, *y*- and *z*-directions may be defined by the

individual ratios S_{outx} / S_{scrx} etc., or else directly by the values elements of $\boldsymbol{S_{out}}$ for the case of unity valued source inputs.

V. Characterizing Sensor Position and Orientation Sensitivity

The model described in section IV is applied to characterize variations in source-sensor coupling for prescribed sensor configurations and position/orientation. Sensor output is calculated by evaluation of (5) according to sensor position (α,β), orientation variables (ψ, θ, ϕ) and system constants (M,r).

A. Sensor Recombination Strategies

The use of multiple source and/or sensor coils requires a strategy for recombining each of the three sensor signal components of $\boldsymbol{S_{out}}$ such that a composite sensor output is produced according to some operation f_c: $S_{out\_comb} = f_c(S_{outx}, S_{outy}, S_{outz})$. Further inspection of (2) shows that if all source/sensor coils are enabled and positioned as per Fig. 3, then the combined summed sensor output is given directly by $S_{out\_comb} = M/r_3(S_{srcx} - 0.5\ S_{srcy} - 0.5\ S_{srcz})$. If each source coil is further assumed to be driven by a normalised voltage of 1V, vector summation of each sensor output would result in net zero output. For this reason tri-source coils considered non-beneficial, and instead a single X-source and tri-sensor arrangement is considered as illustrated in Fig. 3 (d).

There are a number of possible sensor recombination operations f_c, noting further that phase sensitive recombination is limited to the received polarities [0, π].

1) Direct summation:

The simplest recombination approach involves a direct vector summation of each coil output, $S_{out\_comb} = S_{outx} + S_{outy} + S_{outz}$.

2) Rectify-summation:

Rectify-summation involves the simplest practical operation of combining the outputs produced by idealized diodes connected to each sensor output, $S_{out\_comb} = |S_{outx}| + |S_{outy}| + |S_{outz}|$.

3) Best coil selection:

Best coil selection involves detecting and selecting the strongest (absolute) coupled voltage from any single coil for a given position, $S_{out\_comb} = max\ (|S_{outx}|, |S_{outy}|, |S_{outz}|)$.

4) RMS:

The RMS approach applies the expression $S_{out\_comb} = [1/3\ (S_{outx}^2 + S_{outy}^2 + S_{outz}^2)]^{1/2}$, which is proportional to the average coupled power from the tri-sensor.

B. Sensor Coverage

Aside from direct inspection of the resulting combined sensor output for various positions and orientations, a key metric for IIoT applications is sensor coverage, C, which defines the region over which the quality of coupling is sufficient for power and communications. This is defined here as the ratio:

$$C(t) = \frac{\sum_{\alpha,\beta}(|S_{out\_comb}|) \geq t}{4\pi r^2} \tag{7}$$

where t is the threshold value normalized to the maximum sensor output and the summation operator calculates the area over which the absolute sensor output exceeds t. When evaluated over the sphere of radius r, (6) gives the fractional area over which the sensor receives sufficient power and is able to communicate.

C. Non-Symmetrical Coils

Coupling analysis can be extended to account for specific applications restrictions, such as prioritized sensor positions and rotations that are weighted according to their likelihood within the geometry. An example of one such generalization is when the area of each tri-sensor coil is no longer equal, as is seen in modern System-on-Chip (SoC) assembles in which sensors assume a "two-and-a-half-dimensional" (2.5D) form [33]. This modification may be accounted for by consideration of (1) and the previously stated assumption ($a^2 < r^2$): since M is directly proportional to the square of coil radius, sensor sensitivity and therefore relative scaling of the coil area may be applied directly to the components of the output vector $\boldsymbol{S_{out}}$.

VI. Simulation Results and Analysis

Graphical representations of coupling quality were generated by a Matlab script that evaluates (5) over n discrete sensor positions α = [-π...2π/(n-1)... π] and β = [-π/2...π/(n-1)... π/2]. Normalized electrical and separation conditions have been assumed (i.e., M = r = 1).

A. Co-planar coils

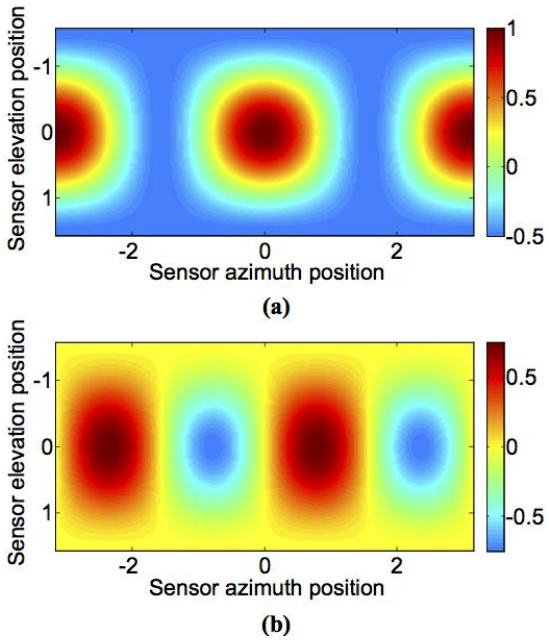

Figure 5. Examples of two-dimensional coupling maps. (a) X-sensor (b) Y-sensor (units in radians).

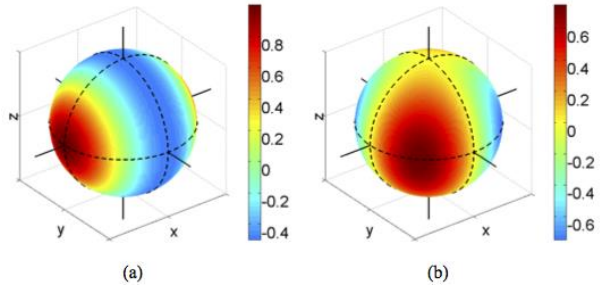

Figure 6. 3D visual maps created by *X*-source and *X*/*Y*-sensor coil coupling. (a) *X*-sensor coupling. (b) *Y*-sensor coupling.

To confirm the basic model, the simplest case of an *X*-source and *X*-sensor coil (see Fig. 3 (a)) was evaluated using *n=200*. The resulting variations of coupling for a single *X*-sensor coil is presented in Fig. 5(a) as a two-dimensional surface representation of coupling quality rendered on a discrete grid comprising 200x200 azimuth and elevation positions. Basic statistical properties summarized in Table I. Regions of weak and null coupling appear in the distribution, severely limiting the useful range of acceptable sensor positions. Adopting instead a single *Y*-sensor coil, similar map of $\boldsymbol{S}_{outy}$ is generated as illustrated in Fig. 5(b). In this case peak, coupling reaches a lower normalized value of 0.75 in comparison to the *X*-sensor case due to the lack of radial field contributions but with a more uniform spread of positive and negative values as indicated by the zero mean value. The result for a single *Z*-sensor coil (not shown) is similar to that of the *Y*-sensor coil.

An alternative visualization of the above results is presented in Fig. 6 wherein the equivalent maps have been superimposed over a spherical shell. The localization of field null regions can immediately be identified as taking the form of circular/elliptical annuli. Such regions exist for all single sensor coil arrangements.

B. Triaxial coil and sensor

The results presented above confirm that singular sensor coil arrangements do not achieve elimination of field coupling nulls. Hence, a single *X*-source and triaxial coil sensor arrangement was adopted. Visual results are presented in Fig. 7 along with key evaluation metrics in Table I. For the direct summation method, field nulls persist around annular regions (Fig. 7a) while the normalized sensor output lies between +1.57 and -1.05 – extended in comparison to the single *X*-source coil due to the additional *Y*- and *Z*-sensor contributions – but accompanied by highly localized regions of strong coupling. This view is supported by low arithmetic mean and high standard deviation values.

Direct summation results in regions of null coupling due to the preservation of phase inversions within the linear summation operation, a problem that is overcome by adopting one of the alternative recombination methods. Comparative results are presented in Fig. 7(b-d) and Table I for each approach. In addition, a direct comparison of the variations in coupling extracted along the equatorial line of the unit sphere is plotted in Fig. 8, where the smoothing effect of the RMS approach is apparent. The best overall

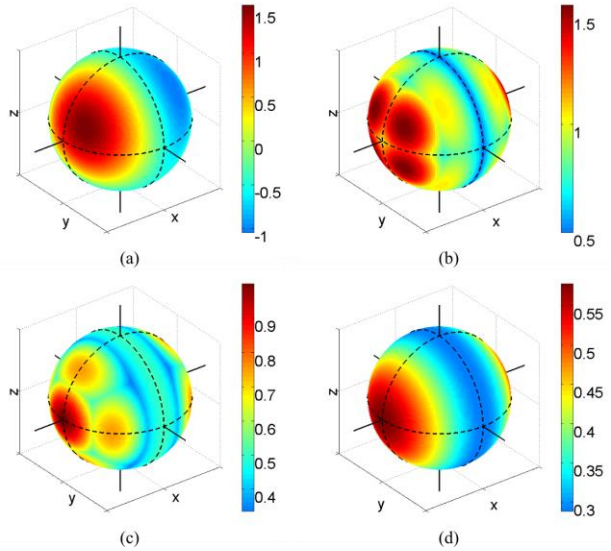

Figure 7. Tri-sensor output produced by various recombination methods and for a single *X*-source coil. (a) Direct summation method. (b) Rectify-summation method. (c) Best coil output selection (based on absolute value). (d) RMS.

performance is seen for the best coil and rectify-sum methods, though these approaches assume that the I-IoT application is tolerant to the more confined regions of strong coupling and rapid variations therein.

TABLE I. STATISTICAL PROPERTIES OF SINGLE OUTPUT COIL AND TRI-COIL RECOMBINATIONS METHODS ACROSS ALL DISCRETE POSITIONS OF A ZERO-ORIENTATION TRI-COIL SENSOR.

	Max	Min	Mean	SD[a]	C[b] (*t*=0.75)
Single *x*-sensor	1.00	-0.50	-0.13	0.42	5.75%
Single *y*-sensor	0.75	-0.75	≈ 0	0.32	12.15%
Single *z*-sensor	0.75	-0.75	≈ 0	0.38	17.08%
Direct-sum	1.55	-1.05	-0.13	0.65	6.10%
Rectify-sum	1.55	0.50	0.93	0.28	21.26%
Best coil	1.00	0.34	0.55	0.13	5.77%
RMS	0.58	0.29	0.37	0.09	25.00%

SD[a] = standard deviation.
C[b] = coverage for specified threshold *t*.

C. Application-Specific Constraints

Given the above characterisation and the chosen arrangement of *X*-source and tri-sensor coils, application-specific considerations may be investigated by applying a series of constraints on the expected coverage *C* threshold coupling quality *t* and position/orientation freedom of the sensor. In this context, *C* is calculated as the percentage area lying on the unit sphere over which *t* is exceeded.

1) Threshold-delimited coverage

Choosing t = 0.75, the cases of a single *Y*-sensor and triaxial coil sensor utilizing the rectify-summation method are visualized in Fig. 9, where the maps have been divided into regions remarking the acceptable/unacceptable sensor positions. Referring again to Table I, the corresponding coverage values show that the rectify-summation method achieves a coverage 1.75x higher than the single *Y*-sensor.

Further comparisons may be drawn from inspection of Table I and evaluation of (5) for different *t*.

2) Restricted sensor position

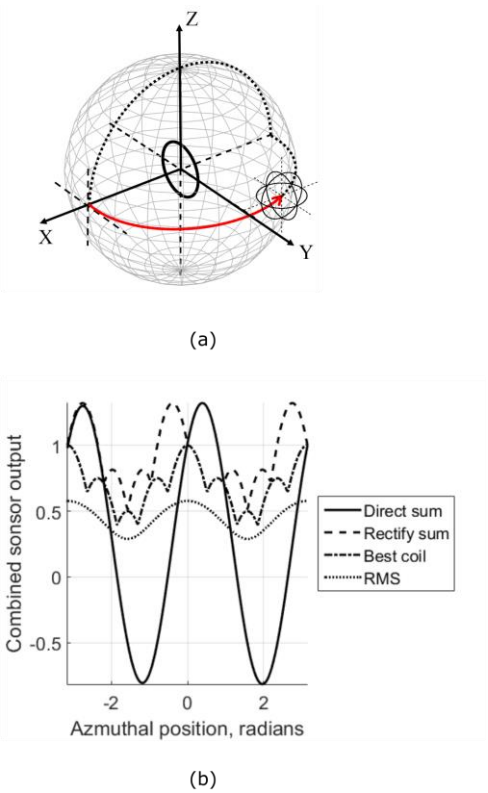

Figure 8. Variations of tri-coil outputs for each recombination method. (a) Diagram showing path traced by tri-coil along the equatorial line. (b) Corresponding plots of recombination outputs for a single *X*-source coil for tri-coil positions around the equatorial line ($-\pi \leq \alpha \leq \pi$, $\beta = 0$).

Choosing once more the rectify-summation method and applying a nominal sensor rotation of $\pi/4$ for each of the rotation directions in turn, the resulting coupling variations are shown visually in Fig. 10. Further insight into the sensitivity to sensor rotation is gained by aggregating the

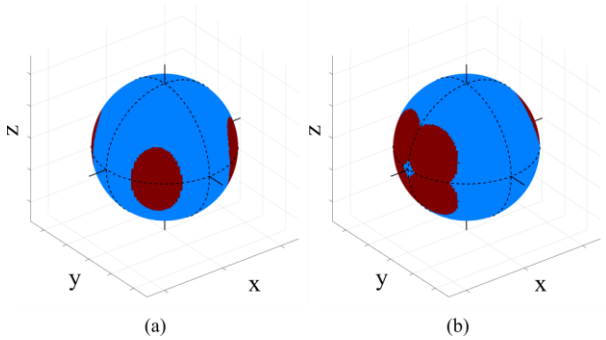

Figure 10. Threshold-delimited coupling maps for (a) single *Y*-sensor and (b) tri-sensor with rectify-summation method. Red shaded regions indicate where the output exceeds 75% of the maximum output; blue shaded regions indicate regions where coupling is insufficient.

coverage results across a range of sensor positions and orientations. An example of this is presented in Fig. 11, for which rotations were applied over the range $[0, \pi]$ and t =

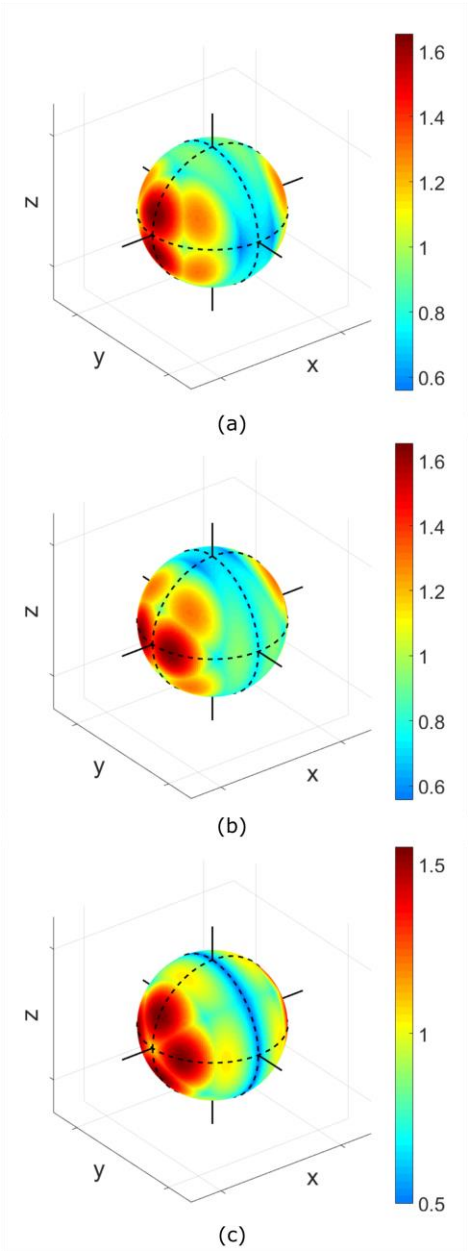

Figure 9. Effect of rotation of triaxial coil. (a) Azimuth rotation by $\pi/4$. (b) Elevation rotation by $\pi/4$. (c) Roll rotation by $\pi/4$.

0.5. For this case, appreciable sensitivity to sensor rotation is observable and maxima for $\psi = \theta = \pi/4$, but a corresponding minimum for the case of roll rotation.

3) Non-equal sensor geometry

Another consideration is the relative area available for each of the triaxial sensor coils, which may be non-identical. A relatively subtle instance of this is visualized in Fig. 12a, in which the area of a *Z*-oriented sensor has been reduced to

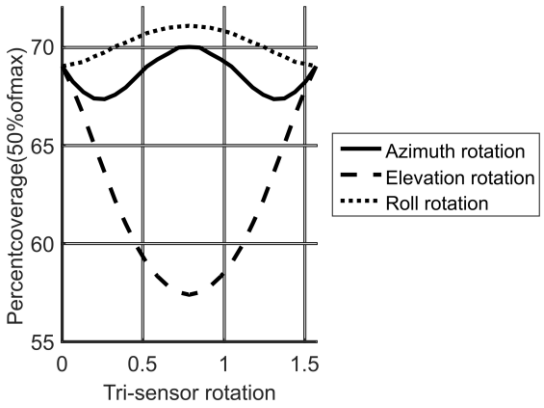

Figure 12. Calculated coverage distributions versus tri-sensor rotation with single X-source coil. For the cases shown, rectify sum sensor recombination is used and a threshold t = 0.5 was specified.

1/3 relative to that of the *X*- and Y-sensors by scaling S_{outz}. In this case the regions of maximal coupling about the *X*-axis become more widely spread (cf. Fig. 7(b)) with potential benefits for some applications. Overall coverage is however reduced by 27% in comparison to the equal-area triaxial sensor. As the sensor orientation is altered the resulting coverage may be evaluated, an example of which is seen in Fig. 12b.

TABLE II. STATISTICAL RESULTS FOR TRI-SENSOR WITH SCALED AND ROTATED Z-COIL USING RECTIFY-SUMMATION METHOD.

	Max	Min	Mean	SD[a]	C[b] (t=0.75)
Z-coil scaled	1.34	0.24	0.73	0.23	15.51%
Z-coil scaled and rotated	1.44	0.21	0.77	0.21	9.32%

SD[a] = standard deviation.
C[b] = coverage for specified threshold *t*.

VII. CONCLUSIONS

The presented position and orientation coupling model permits detailed investigation of arbitrary single, dual- and tri-coil source/sensor configurations including sensor recombination methods, from which the rectify-summation method was favoured for its ease of implementation and high coverage. Evaluation procedures based on the threshold-delimited coverage metric were demonstrated in the context of numerous configurations including non-equal sensor area and restricted position/orientation. From this, a design procedure for analysing new applications was suggested.

The inclusion of tri-sensor coils brings significant improvements to the robustness of source-sensor coupling – a necessary property for delivering high quality, robust data to future IIoT applications.

Since coverage tends to remain clustered around regions aligned with the orientation of the source coil, tri-source coils could be considered provided that a time-multiplexed switching scheme were employed to avoid severe coupling nulls. The model could be extended to include close proximity coupling ($a \approx r$), though the inclusion of all near-field effects is a complex task. A further extension of this work will consider combined 3D additive fabrication of tri-sensor support structures and conductive tracks and their subsequent integration into complex systems infrastructures.

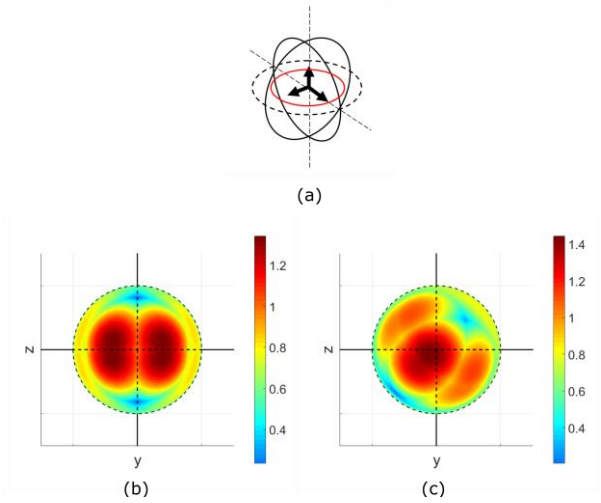

Figure 11. Example of triaxial coil coupling wherein the *Z*-oriented coil is 33% smaller than the *X*- and *Y*-oriented coils. (a) Tri-axial sensor geometry reduction in size of *Z*-sensor coil in relation to *X*- and *Y*- sensor coils. (b) Coupling variation using the rectify-summation method and zero-orientation *X*-source coil (c) Equivalent coupling variation for rotated sensor ($\psi = \pi/8$, $\phi = \pi/4$, $\theta = -\pi/8$)

Since coverage tends to remain clustered around regions aligned with the orientation of the source coil, tri-source coils could be considered provided that a time-multiplexed switching scheme were employed to avoid severe coupling nulls. The model could be extended to include close proximity coupling ($a \approx r$), though the inclusion of all near-field effects is a complex task. A further extension of this work will consider combined 3D additive fabrication of tri-sensor support structures and conductive tracks and their subsequent integration into complex systems infrastructures.

ACKNOWLEDGMENT

This work was supported by the UK EPSRC Centre for Innovative Manufacturing in Through-life Engineering Services (EP/I033246/1).

REFERENCES

[1] L. D. Xu, W. He, and S. Li, "Internet of Things in Industries: A Survey," *IEEE Trans. Ind. Inform.*, vol. 10, no. 4, pp. 2233–2243, Nov. 2014.

[2] Z. Pang, Q. Chen, W. Han, and L. Zheng, "Value-centric design of the internet-of-things solution for food supply chain: Value creation, sensor portfolio and information fusion," *Inf. Syst. Front.*, vol. 17, no. 2, pp. 289–319, Aug. 2012.

[3] P. Barnaghi, A. Sheth, V. Singh, and M. Hauswirth, "Physical-Cyber-Social Computing: Looking Back, Looking Forward," *IEEE Internet Comput.*, vol. 19, no. 3, pp. 7–11, May 2015.

[4] T. S. Baines, H. W. Lightfoot, O. Benedettini, and J. M. Kay, "The servitization of manufacturing: A review of literature and reflection

on future challenges," *J. Manuf. Technol. Manag.*, vol. 20, no. 5, pp. 547–567, Jun. 2009.

[5] J. Lee, J. Ni, D. Djurdjanovic, H. Qiu, and H. Liao, "Intelligent prognostics tools and e-maintenance," *Comput. Ind.*, vol. 57, no. 6, pp. 476–489, Aug. 2006.

[6] L. Atzori, A. Iera, and G. Morabito, "The Internet of Things: A survey," *Comput. Netw.*, vol. 54, no. 15, pp. 2787–2805, Oct. 2010.

[7] C. Wang, Z. Bi, and L. D. Xu, "IoT and Cloud Computing in Automation of Assembly Modeling Systems," *IEEE Trans. Ind. Inform.*, vol. 10, no. 2, pp. 1426–1434, May 2014.

[8] I. Lee and K. Lee, "The Internet of Things (IoT): Applications, investments, and challenges for enterprises," *Bus. Horiz.*, vol. 58, no. 4, pp. 431–440, Jul. 2015.

[9] J. J. M. Seddon and W. L. Currie, "Cloud computing and trans-border health data: Unpacking U.S. and EU healthcare regulation and compliance," *Health Policy Technol.*, vol. 2, no. 4, pp. 229–241, Dec. 2013.

[10] Y. Kawamoto, H. Nishiyama, N. Kato, N. Yoshimura, and S. Yamamoto, "Internet of Things (IoT): Present State and Future Prospects," *IEICE Trans. Inf. Syst.*, vol. E97-D, no. 10, pp. 2568–2575, Oct. 2014.

[11] R. McWilliam, S. Khan, and A. Purvis, "Modelling the Positional and Orientation Sensitivity of Proximity Sensors for Industrial IoT," in *UKSim-AMSS 18th International Conference on Mathematical Modelling & Computer Simulation*, Cambridge, UK, 2016, pp. 355–360.

[12] H. Ning and Z. Wang, "Future Internet of Things Architecture: Like Mankind Neural System or Social Organization Framework?," *IEEE Commun. Lett.*, vol. 15, no. 4, pp. 461–463, Apr. 2011.

[13] Z. Pang, Q. Chen, J. Tian, L. Zheng, and E. Dubrova, "Ecosystem analysis in the design of open platform-based in-home healthcare terminals towards the internet-of-things," in *Advanced Communication Technology (ICACT), 2013 15th International Conference on*, 2013, pp. 529–534.

[14] K. Finkenzeller, *RFID Handbook: Fundamentals and Applications in Contactless Smart Cards, Radio Frequency Identification and Near-field Communication*, 3rd Edition edition. Chichester, West Sussex ; Hoboken, NJ: Wiley-Blackwell, 2010.

[15] X. Mou and H. Sun, "Wireless Power Transfer: Survey and Roadmap," in *Vehicular Technology Conference (VTC Spring), 2015 IEEE 81st*, 2015, pp. 1–5.

[16] Z. Hajduk, B. Trybus, and J. Sadolewski, "Architecture of FPGA Embedded Multiprocessor Programmable Controller," *IEEE Trans. Ind. Electron.*, vol. 62, no. 5, pp. 2952–2961, May 2015.

[17] B. Martinez, M. Monton, I. Vilajosana, and J. D. Prades, "The Power of Models: Modeling Power Consumption for IoT Devices," *IEEE Sens. J.*, vol. 15, no. 10, pp. 5777–5789, Oct. 2015.

[18] J. M. Tien, "Internet of connected ServGoods: Considerations, consequences and concerns," *J. Syst. Sci. Syst. Eng.*, vol. 24, no. 2, pp. 130–167, May 2015.

[19] N. Mishra, C.-C. Lin, H.-T. Chang, N. Mishra, C.-C. Lin, and H.-T. Chang, "A Cognitive Adopted Framework for IoT Big-Data Management and Knowledge Discovery Prospective, A Cognitive Adopted Framework for IoT Big-Data Management and Knowledge Discovery Prospective," *Int. J. Distrib. Sens. Netw.*, vol. 2015, 2015, p. e718390, Oct. 2015.

[20] S. Andreev, O. Galinina, A. Pyattaev, M. Gerasimenko, T. Tirronen, J. Torsner, J. Sachs, M. Dohler, and Y. Koucheryavy, "Understanding the IoT connectivity landscape: a contemporary M2M radio technology roadmap," *IEEE Commun. Mag.*, vol. 53, no. 9, pp. 32–40, Sep. 2015.

[21] T. Heikkilä, E. Strömmer, S. Kivikunnas, M. Järviluoma, M. Korkalainen, V. Kyllönen, E. Sarjanoja, and I. Peltomaa, "Low intrusive Ehealth monitoring: human posture and activity level detection with an intelligent furniture network," *IEEE Wirel. Commun.*, vol. 20, no. 4, pp. 57–63, Aug. 2013.

[22] N. Li, W. Yi, Z. Bi, H. Kong, and G. Gong, "An optimisation method for complex product design," *Enterp. Inf. Syst.*, vol. 7, no. 4, pp. 470–489, Nov. 2013.

[23] T. Vollmer, M. Manic, and O. Linda, "Autonomic Intelligent Cyber-Sensor to Support Industrial Control Network Awareness," *IEEE Trans. Ind. Inform.*, vol. 10, no. 2, pp. 1647–1658, May 2014.

[24] Z. Bi, "Revisiting System Paradigms from the Viewpoint of Manufacturing Sustainability," *Sustainability*, vol. 3, no. 9, pp. 1323–1340, Aug. 2011.

[25] C. Alcaraz, R. Roman, P. Najera, and J. Lopez, "Security of industrial sensor network-based remote substations in the context of the Internet of Things," *Ad Hoc Netw.*, vol. 11, no. 3, pp. 1091–1104, May 2013.

[26] D. Bandyopadhyay and J. Sen, "Internet of Things: Applications and Challenges in Technology and Standardization," *Wirel. Pers. Commun.*, vol. 58, no. 1, pp. 49–69, Apr. 2011.

[27] G. Gupta, B. P. Singh, A. Bal, D. Kedia, and A. R. Harish, "Orientation Detection Using Passive UHF RFID Technology [Education Column]," *IEEE Antennas Propag. Mag.*, vol. 56, no. 6, pp. 221–237, Dec. 2014.

[28] P. Wei, W. Che, Z. Bi, C. Wei, Y. Na, L. Qiang, and M. Hao, "High-Efficiency Differential RF Front-End for a Gen2 RFID Tag," *IEEE Trans. Circuits Syst. II Express Briefs*, vol. 58, no. 4, pp. 189–194, Apr. 2011.

[29] X. Qing and Z. N. Chen, "Proximity Effects of Metallic Environments on High Frequency RFID Reader Antenna: Study and Applications," *IEEE Trans. Antennas Propag.*, vol. 55, no. 11, pp. 3105–3111, Nov. 2007.

[30] S. Sasaki, T. Seki, K. Imanaka, M. Kimata, T. Toriyama, T. Miyano, and S. Sugiyama, "Batteryless-Wireless MEMS Sensor System with a 3D Loop Antenna," in *2007 IEEE Sensors*, 2007, pp. 252–255.

[31] C. Kruesi, R. Vyas, and M. Tentzeris, "Design and Development of a Novel 3-D Cubic Antenna for Wireless Sensor Networks (WSNs) and RFID Applications," *IEEE Trans. Antennas Propag.*, vol. 57, no. 10, pp. 3293–3299, Oct. 2009.

[32] F. H. Raab, E. B. Blood, T. O. Steiner, and H. R. Jones, "Magnetic Position and Orientation Tracking System," *IEEE Trans. Aerosp. Electron. Syst.*, vol. AES-15, no. 5, pp. 709–718, Sep. 1979.

[33] R. R. Tummala, "SOP: what is it and why? A new microsystem-integration technology paradigm-Moore's law for system integration of miniaturized convergent systems of the next decade," *IEEE Trans. Adv. Packag.*, vol. 27, no. 2, pp. 241–249, May 2004.